Aggregation properties and structural studies of anticancer drug Irinotecan in DMSO solution based on NMR measurements

ARTICLE *in* JOURNAL OF MOLECULAR STRUCTURE · APRIL 2012

Impact Factor: 1.6 · DOI: 10.1016/j.molstruc.2012.01.012

7 AUTHORS, INCLUDING:

Vincent Aroulmoji
Mahendra Engineering College
78 PUBLICATIONS **241** CITATIONS
SEE PROFILE

Gowtha N Sundaraganesan
Annamalai University
136 PUBLICATIONS **2,340** CITATIONS
SEE PROFILE

Journal of Molecular Structure 1013 (2012) 26–35

Contents lists available at SciVerse ScienceDirect

Journal of Molecular Structure

journal homepage: www.elsevier.com/locate/molstruc

Aggregation properties and structural studies of anticancer drug Irinotecan in DMSO solution based on NMR measurements

N. D'Amelio [a,b,*], V. Aroulmoji [c], A. Toraldo [a], N. Sundaraganesan [d], P.M. Anbarasan [e]

[a] Bracco Imaging SpA-CRB Trieste, AREA Science Park, Building Q, SS 14, Km 163.5, 34149 Basovizza, Trieste, Italy
[b] CBM S.r.l. – Consorzio per il Centro di Biomedicina Molecolare, AREA Science Park, SS 14, Km 163.5, 34149 Basovizza, Trieste, Italy
[c] Advanced Research Centre for Health, Environment and Space (ARCHES), Via Giuseppe Leuzzi 18, I-70013 Castellana Grotte, Italy
[d] Department of Physics (Engg.), Annamalai University, Annamalai Nagar 608 002, India
[e] Department of Physics, Periyar University, Salem 636 011, India

ARTICLE INFO

Article history:
Received 28 September 2011
Received in revised form 12 January 2012
Accepted 12 January 2012
Available online 20 January 2012

Keywords:
NMR
Irinotecan
Aggregation
Diffusion
DMSO

ABSTRACT

Irinotecan is an antitumor drug mostly used in the treatment of colorectal cancer. Its efficacy is influenced by the chemical state of the molecule undergoing chemical equilibria, metabolic changes and photodegradation. In this work, we describe the chemical equilibria of the drug in dimethyl sulfoxide (DMSO). The energetic barrier for hindered rotation around the bond connecting the piperidino—piperidino moiety with the camptothecin-like fragment was evaluated. Furthermore, we showed how the molecule aggregates in DMSO solution forming dimeric species able to prevent its degradation. The equilibrium constant for self-aggregation was determined by NMR based on the assumption of the isodesmic model. The formation of a dimer was highlighted by NMR diffusion ordered spectroscopy (NMR-DOSY) experiments at the concentrations used. Structural features of the complex were inferred by NOE and ^{13}C chemical shift data. Molecular modelling of the complex driven by experimental data, lead to a structure implying the formation of two hydrogen bonds involving the lactone ring whose opening is one of the main causes of drug degradation. This species is probably responsible for the improved stability of the drug at concentrations higher than 1 mM.

1. Introduction

Irinotecan (7-ethyl-10-[4-(1-piperidino)-1-piperidino]carbonyloxycamptothecin also called CPT-11) is an antitumor drug mainly used in the treatment of colorectal cancer [1,2], although it has been used in the treatment of other cancers (such as small lung cancer [3]). Its chemical structure is the synthetic analogue of the natural alkaloid camptothecin (CPT), a molecule extracted from the Chinese tree *Camptotheca Acuminata* [4] or different sources [5].

Irinotecan is obtained by chemical modification of camptothecin with the aim of increasing its intrinsically low water solubility. The molecule is subministered essentially as a pro-drug as it undergoes enzymatic cleavage of the bispiperidino-side chain by carboxylesterase to form 7-ethyl-10-hydroxycamptothecin (SN-38) [6–8], a potent topoisomerase I inhibitor. CPT analogues stabilize the complex between topoisomerase and DNA, thus preventing its unwinding during replication and leading to cell death [9–11].

The action of the carboxyesterase is inhibited by the opening of the lactone ring (also referred to as "e" ring) generating the carboxylate form in camptothecin derivatives [12–15]. The chemical equilibrium is reversible and dependent on pH (with the open form favoured at neutral and acidic pHs) [16–20]. In vivo, the equilibrium is further shifted to the inactive form due to its association of plasma proteins [21,22].

In order to solve this problem, limiting the efficacy of the drug, different delivery systems has been proposed in the effort of preventing the lactone opening [23–27]. Such systems have also been used to limit the toxicity by controlled release [28–32].

The structural basis mechanism of action is quite well understood, thanks to crystallographic and NMR data. The structure of CPT and its analogues was investigated by NMR and computational methods [33] also in its DNA binding properties [34]. The X-ray structure of the complex topoisomerase-DNA has been solved both in the presence of captothecin and its topotecan analogue [35,36]. In the case of topotecan the crystal structure has been solved in complex with two topoisomerase mutants [37] showing drug resistance. In addition, a solution structure of the complex of topotecan with nicked DNA (the form present in the complex with topoisomerase) has been proposed by NMR and molecular modelling, showing small differences with the crystallographic structure

* Corresponding author. Present address: Centro Nacional de Investigaciones Oncológicas, Computational Biophysics Group, C/Melchor Fernández Almagro, 3, 28029 Madrid, Spain. Tel.: +34 917328000x3081.
E-mail address: ndamelio@cnio.es (N. D'Amelio).

0022-2860/$ - see front matter © 2012 Elsevier B.V. All rights reserved.
doi:10.1016/j.molstruc.2012.01.012

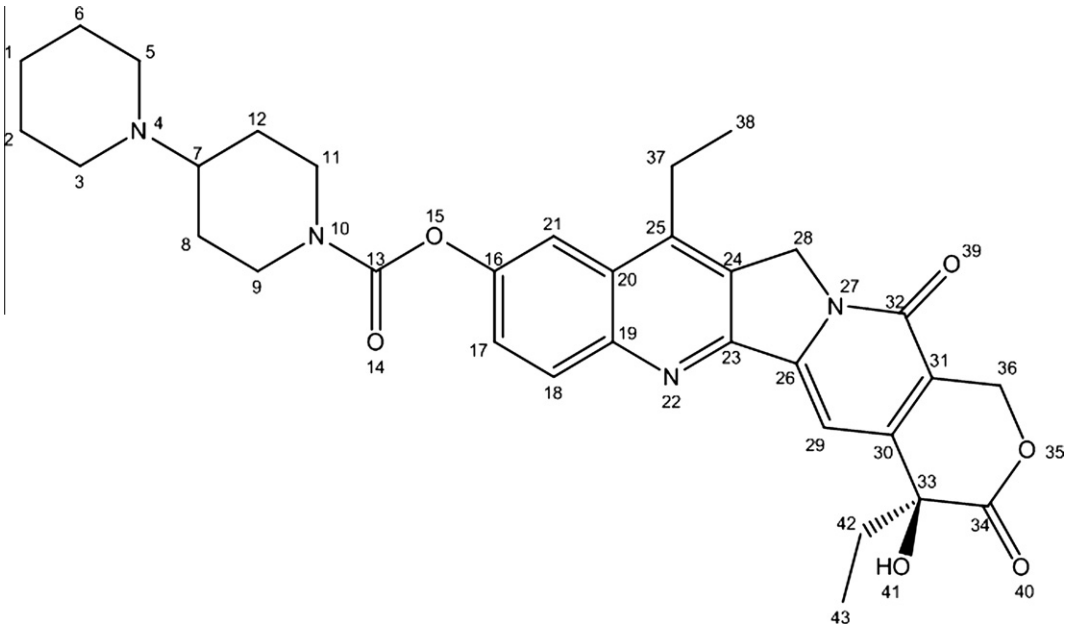

Scheme 1. Molecular structure of Irinotecan. Figure was created using Chem Draw Ultra 11.0.1.

[15]. The structure of rabbit liver carboxylesterase with 4-piperidino–piperidine (one of the product of the activation reaction of Irinotecan by carboxyesterase) has been solved by X-ray studies [38]. Finally, the crystallographic structure of Irinotecan with Torpedo californica acetylcholinesterase demonstrates the causes of its cholinergic syndrome side effect [39].

Irinotecan is reported to degrade in a variety of conditions. The main metabolites formed in vivo in patients body fluids were identified [32]. Additionally the drug undergoes degradation in aqueous solutions [20,40,41]. Self association has been reported both in aqueous solutions [42] and in the presence of liposomes [31] giving rise to helical shaped aggregates implying aromatic ring stacking. The aggregates in water are mainly formed by dimers while aggregation was not reported in different organic solvents [42].

In this work, we characterized the aggregation phenomenon of Irinotecan in DMSO solution. Our data suggest a possible mechanism preventing drug degradation through the formation of multimeric species. The association constant was determined by NMR using the isodesmic model; the number of particles per aggregate was estimated by diffusion measurements demonstrating the formation of dimers at concentrations above 1 mM. Molecular modelling based on experimental NMR data suggest the formation of intermolecular hydrogen bonds involving the lactone ring whose opening is one of the main causes of drug degradation. For this reason, the structural details of the model might able to explain why the formation of dimers prevents Irinotecan degradation in concentrated solutions. Interestingly, pharmaceutical formulations in water are prepared at a concentration (about 30 mM) which could possibly benefit of this kind of interaction for their stability.

2. Experimental

The compound Irinotecan was purchased from Fermion, Finland and used as such without any further purification.

2.1. NMR experiments

Unless otherwise specified, all experiments were carried out at 300 K on a Bruker Avance III Ultra Shield Plus 600 MHz spectrometer provided with a two channel BBI probe, using concentrations ranging from 12.5 μM to 20 mM in d_6-DMSO. Residual DMSO signal was used for chemical shift referencing, as TSP (trimethylsilyl propionate) was shown to be unreliable, causing the shift of all other peaks by similar amounts. Even if DMSO signal may change its position due to its interaction with Irinotecan, this shift cannot be larger than few tens of ppb at the concentrations used. Hydrogen and carbon assignment was accomplished by a series of 2D spectra, namely: 2D-NOESY, 2D-COSY, 2D-ROESY, 2D-^{1}H, ^{1}H-TOCSY, 2D-^{1}H, ^{13}C HSQC, and 2D-^{1}H, ^{13}C-HMBC.

Diffusion coefficients were calculated by measuring the intensity of the signals as a function of the gradient strength G and performing regression analysis with the equation [43]:

$$I = I_0 \exp\left[-Dq^2(\Delta - \delta/3 - \tau/2)\right] \quad (1)$$

where I and I_0 are the intensities of the signal for each gradient strength used in the experiment and for 2% gradient strength respectively, Δ and δ are the big and the little delta of the BPP-LED experiment, τ is the gradient pulse separation and $q = 2\pi\gamma G\delta$.

The apparent molecular weight M was calculated as [44,45]:

$$M = \left(\frac{k_B T}{6\eta\pi F D}\right)^3 \left[\frac{4\pi N_A}{3(\upsilon_2 + \delta_1\upsilon_1)}\right] \quad (2)$$

where, T is the absolute temperature, η is the viscosity of the solution, K_B is the Boltzmann constant, N_A is Avogadro's number, v_2 and v_1 are the partial specific volumes of the molecule and solvent water, respectively, and δ_1 is the fractional amount of solvent bound to the molecule (solvation number). F is the shape factor or Perrin factor, which is defined as the ratio of the friction coefficient of the molecule to that of a hard sphere with equivalent mass and partial specific volume. As for the values of the partial specific volumes v_2 and v_1, 0.73×10^{-6} m^3 g^{-1} and 0.91×10^{-6} m^3 g^{-1} were used for Irinotecan and the solvent [46]. The solvation number δ_1 ranges between 0.3 and 0.4 g of H_2O per gram of solute [45]. For DMSO the lower value was opportunely modified accounting for the difference in molecular weight and volume between the two solvents (water and DMSO). In particular, we multiplied by the ratio MW_{DMSO}/MW_{H2O} and further divided by 2, assuming that one molecule of DMSO is able to displace two water molecules; we obtained a final value of 0.65 g of DMSO per gram of molecule.

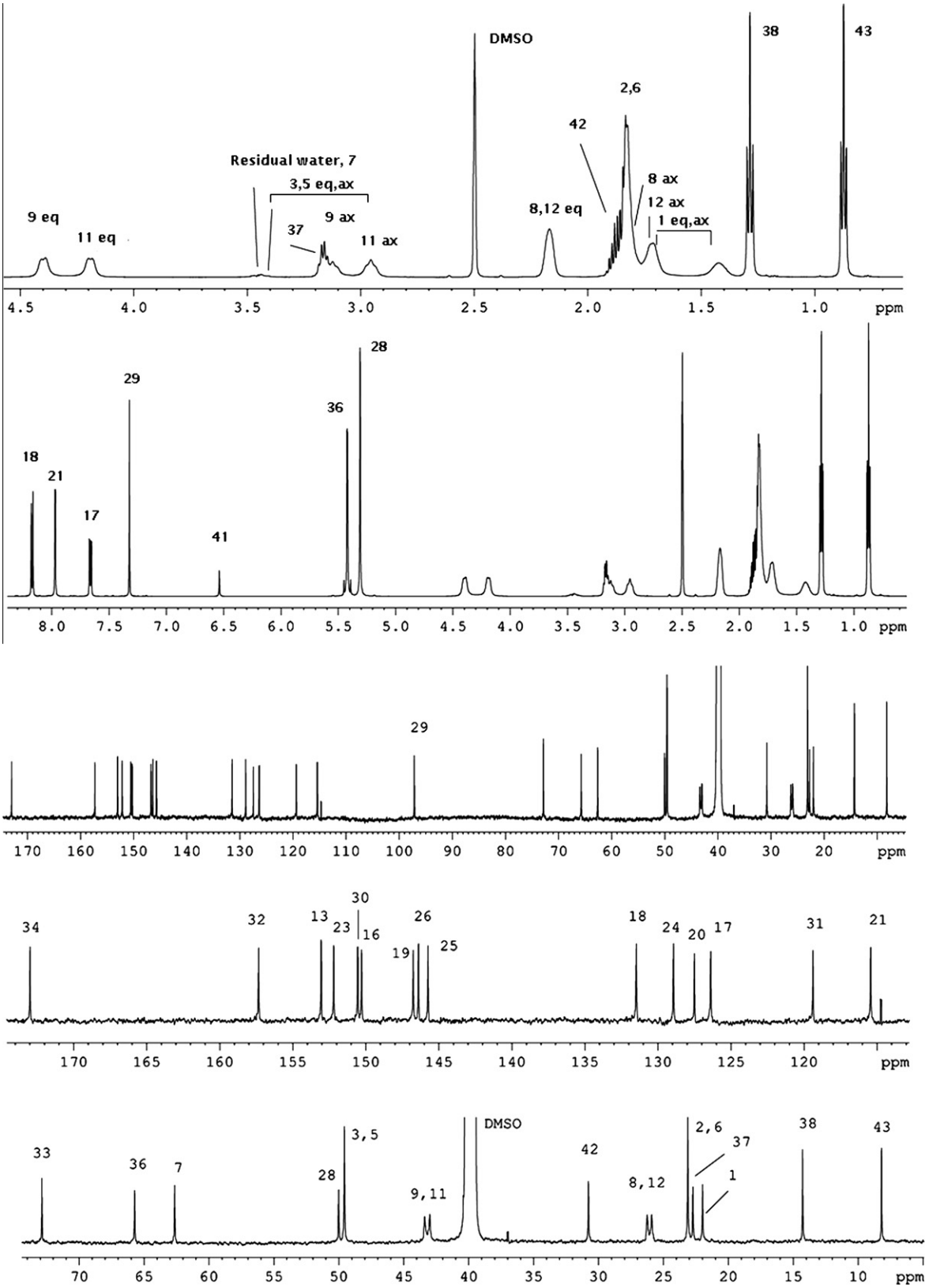

Fig. 1. ^{1}H (top) and ^{13}C (bottom) NMR spectra of Irinotecan 20 mM in d^{6}-DMSO. Figure was created using Bruker program XWINPLOT.

While the molecular weight is not extremely dependent of the solvation number, the shape factor (related to the axial ratio) is more critical and cannot be estimated with precision by molecular modelling due to the flexibility of the bis-piperidino moiety. For this reason, we calibrated its value (1.15 corresponding to an axial ratio of 0.28) from the diffusion coefficient at the lowest concentration on the basis of the expected molecular weight of the monomer (the association constant measured in the present work ensures

Table 1
^{1}H and ^{13}C NMR chemical shifts of Irinotecan 20 mM in d^6-DMSO, T = 300 K.

Atom number	^{1}H chemical shift (ppm)	J coupling (Hz)	^{13}C chemical shift (ppm)
1	1.71; 1.40		21.65
2,6	1.83		22.78
3,5	3.40; 2.97		49.27
7	3.45		62.28
8[a]	2.18 (eq); 1.72 (ax)		25.92
9[a]	4.40 (eq); 3.15 (ax)	^{2}J = 13.4	42.64
11[a]	4.20 (eq); 2.96 (ax)	^{2}J = 13.4	43.05
12[a]	2.18 (eq); 1.82 (ax)		25.58
13			152.73
16			149.94
17	7.67	J_{17-18} = 9.5; J_{17-21} = 2.8	126.05
18	8.17	J_{18-17} = 9.5; J_{18-21} = 1.3	131.15
19			146.4
20			127.17
21	7.98	J_{21-17} = 2.8; J_{21-18} = 1.3	115.11
23			151.86
24			128.16
25			145.39
26			146.16
28	5.31		49.71
29	7.32		96.83
30			150.2
31			119.06
32			156.98
33	3.17		72.53
34			172.65
36	5.43		65.37
37	3.17	J_{37-38} = 7.9	22.38
38	1.29	J_{38-37} = 7.9	13.94
41	6.54		
42	1.87	J_{42-43} = 7.2; ^{2}J = 14.2	30.43
43	0.87	J_{43-42} = 7.2	7.87

[a] The assignment is temptative. 9 could be exchanged with 11 and 8 with 12.

that the amount of dimer is largely negligible at 12.5 μM). As the molecule aggregates, the value is likely to change but in the case of a dimer the flexibility of the bis-piperidino moiety is reduced and a value close to 0.5 can be estimated (see the molecular modelling of the dimer in Section 3.6).

2.2. Mass spectrometry and HPLC

Electrospray ionization mass spectrometry (ESI-MS) was performed using an ion trap mass spectrometer (model LCQ DecaXP Plus, ThermoFinnigan, San Jose, CA, USA), operating in positive and in negative ionization mode (±4.5 kV). The sheath gas (N_2) was typically equal to 0.23 L/min, the temperature of heated capillary was set at 240 °C.

High performance liquid chromatography coupled with UV and mass spectrometry detector (HPLC–UV–MS) was carried out upon connecting the mass spectrometer to a Surveyor ThermoFinnigan HPLC system, equipped with a MS pump, an autosampler and a PDA detector. XCalibur (ThermoFinnigan) data system software (version 1.4) allowed the instruments control as well as data acquisition and processing.

HPLC–MS studies were carried out using a Luna NH_2 column (3.0 ∗ 250 mm, 5 u, 100 Å) from Phenomenex. Separations were performed at 60 °C (flow: 300 μL/min; injection volume: 10 μL) applying the following gradient of CH_3CN in water: 10% (up to 8 min), 40 (up to 13 min), 90 (up to 32 min), 10 (up to 45 min). Electrospray mass spectrometry was carried out using both total ion current (TIC) and single ion monitoring (SIM), set at m/z equal to 587.3 ($[MH]^+$ of Irinotecan). UV detection was performed at 195 nm and 260 nm.

Irinotecan solutions for degradation studies were prepared in DMSO at concentration 0.1 mM.

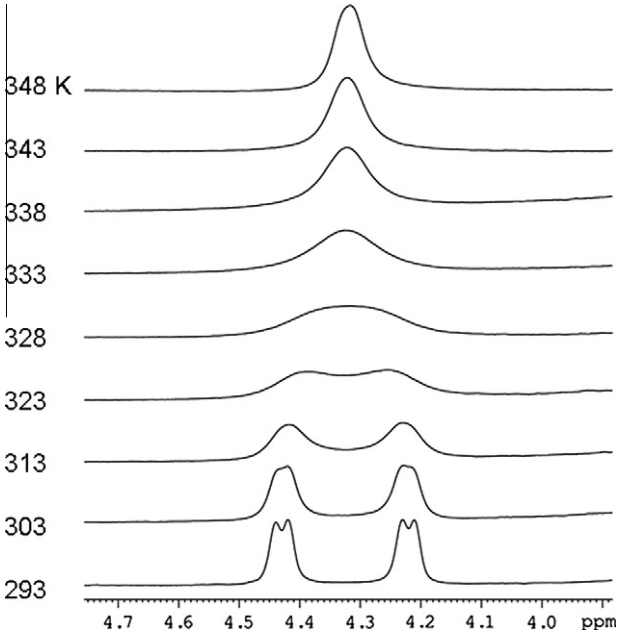

Fig. 2. Temperature dependence of 9, 11 (equatorial protons) in Irinotecan 12.5 mM in DMSO. Figure was created using Bruker program XWINPLOT.

2.3. Structure calculation

NOESY NMR experiments were recorded at 600 MHz on Irinotecan 20 mM in d^6-DMSO. NOESY mixing time was kept long (300 ms) in order to ensure magnetization transfer even in the

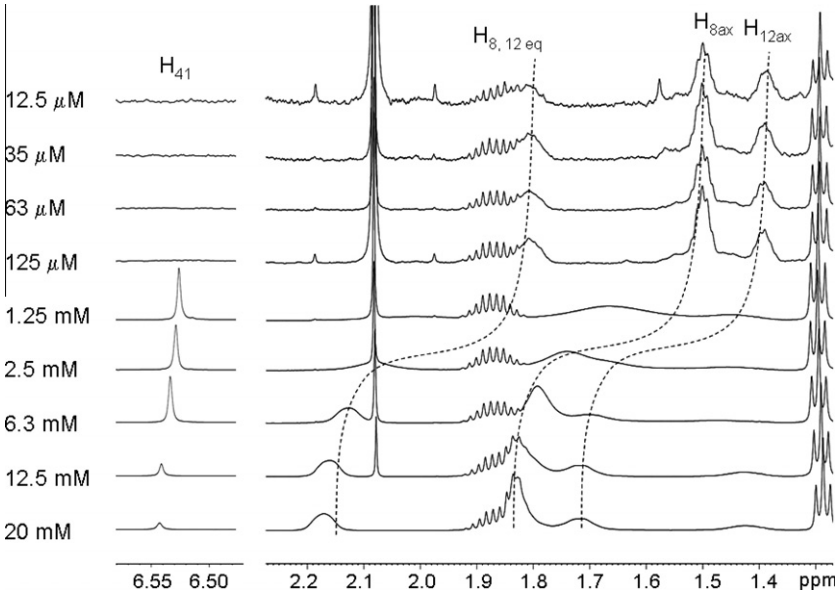

Fig. 3. Concentration dependence of ^{1}H NMR spectra of Irinotecan in DMSO, T = 300 K (selected regions). In the left panel the signal from the exchangeable proton H41 is shown. Figure was created using Bruker program XWINPLOT.

presence of chemical exchange. Spin diffusion can be neglected for most of the rigid parts of the molecule (but not all, see Section 3.6), where protons are far apart for each other; finally the NOE transfer is not very efficient for molecules of the size of Irinotecan, at least at 600 MHz.

The cross peak between protons 17 and 18 was chosen as internal reference volume as the two nuclei are at fixed distance (0.245 nm). Using the reference volume we were able to calculate all other distances as follows:

$$dist = dist^{ref}\sqrt[6]{\frac{V^{ref}}{V}} \quad (3)$$

where $dist^{ref}$ is the interproton distance between protons 17 and 18 (0.245 nm) and V^{ref} is the volume of their NOE cross-peak.

Molecular modelling and. energy minimization were performed using molecular mechanics with MM+ force field [47]. Multiple solutions were generated starting by different relative orientation of each molecule in the dimer. The shielding/deshielding effect on ^{13}C spectra upon increasing drug concentration was interpreted as due to the magnetic anisotropy of Irinotecan aromatic rings and used to select the best model.

3. Results and discussion

The molecular structure of Irinotecan is shown in Scheme 1 with atomic numbering and letters identifying its aromatic rings.

3.1. ^{1}H and ^{13}C NMR assignment

^{1}H and ^{13}C NMR spectra of Irinotecan 20 mM in d^{6}-DMSO are shown in Fig. 1.

Signal assignments were carried out by multidimensional NMR experiments, namely: 2D-^{1}H,^{13}C-HSQC, 2D-^{1}H,^{13}C-TOCSY-HSQC, 2D-^{1}H,^{13}C-HMBC, 2D-^{1}H,^{1}H-COSY and 2D-^{1}H,^{1}H-NOESY. Signal labels follow the atomic numbering shown in Scheme 1; values are reported in Table 1.

Atoms in 9 and 11 positions (and 8, 12 positions) appear not equivalent and this is probably due to the partial double bond character of the amidic bond connecting the piperidino—piperidino moiety to the camptothecin-like fragment. In fact when the rotation is blocked the positions display different chemical environments. Discrimination between the two is only temptative and was based on the fact that position 9 is closer than 11 to the deshielding region of the nearby carbonyl. However, no experiment was able to confirm this assignment.

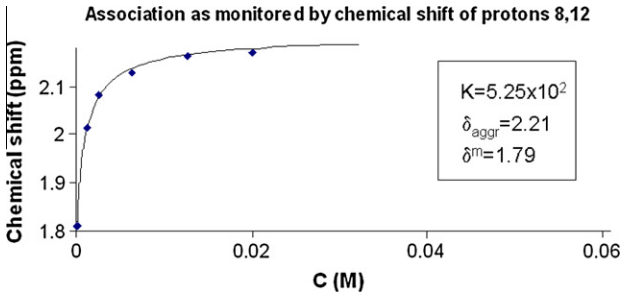

Fig. 4. Equilibrium constant for self association as derived from the isodesmic model using the shifts of protons 8, 12 in Irinotecan. Figure was created using Microsoft Excel 2003.

J coupling constants were measured using a 2D-J resolved spectrum. Discrimination between equatorial and axial protons in position 9, 11 was based on the shape of the signal resulting from different sets of coupling constants. Both the equatorial and the axial protons are split by the large geminal coupling (13.4 Hz) but the axial proton is further split by one large anti ^{3}J coupling with the neighbouring axial protons in positions 8, 12 making it appears as a large triplet. On the contrary, the equatorial proton is split by two small ^{3}J couplings and appears as a large doublet. Due to the large line width, the exact value of the couplings was not measured but the intensity of COSY peaks was used to assign the equatorial and axial protons in positions 8, 12 (axial–axial coupling giving higher intensity).

3.2. Temperature effect on chemical shift: Energetic barriers

As stated above, protons 9 and 11 are subject to chemical equilibrium as their signals (both the equatorials and axials)

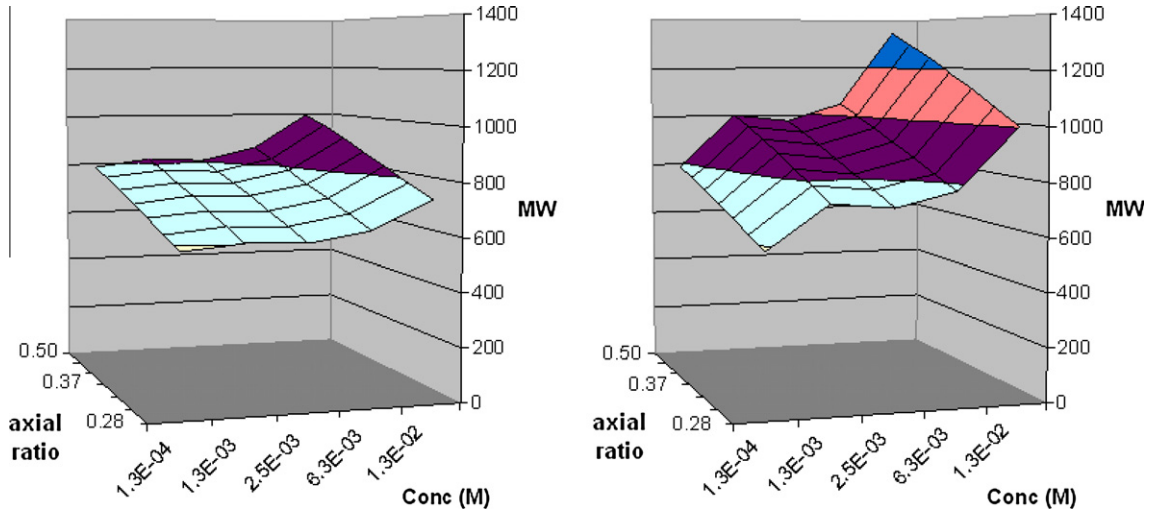

Fig. 5. Average molecular weight of Irinotecan species as a function of concentration and axial ratio as calculated by Eq. (2) using (left) measured diffusion coefficient and (right) diffusion coefficients of the associated form calculated by Eq. (9). Figure was created using Microsoft Excel 2003.

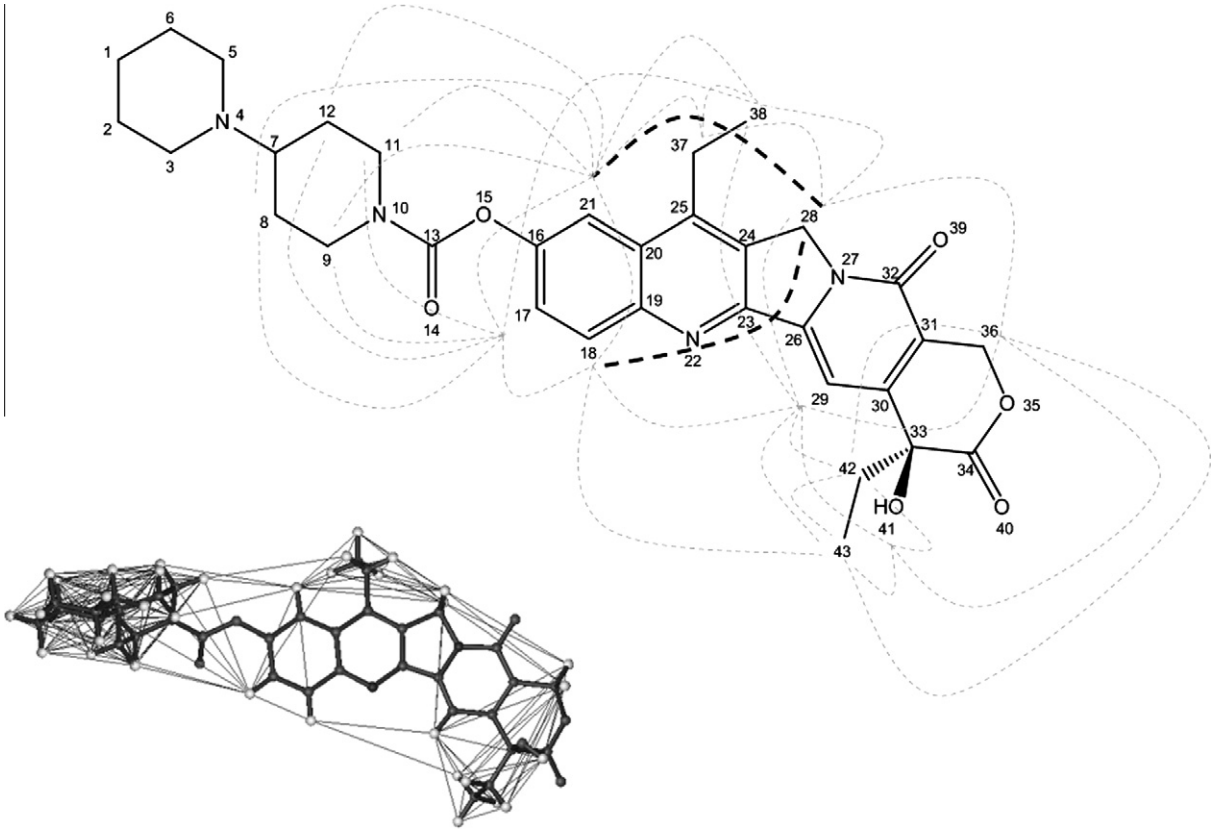

Fig. 6. (top) Proton–proton NOE effects for Irinotecan 20 mM in DMSO and (bottom) interproton distances shorter than 0.55 nm in the monomer. Cross peaks between protons at distance longer than 0.55 nm in the monomer (in bold) could originate from intermolecular effects in the dimeric form of Irinotecan. Figure was created using MOLMOL 2 K.2 and Microsoft Powerpoint 2003.

merge above 323 K. The equilibrium is likely to reflect the "*cis–trans*" isomerisation of the amidic bond adjacent to the carbonyl in position 13 (with a partial double bond character) making the rotation hindered. Fig. 2 shows the temperature dependence of the equatorial protons in position 9, 11; the experiment can reveal the thermodynamics of rotational barriers as at coalescence there is a well definite relationship between the exchange time τ_M and the frequency difference in chemical shift Δv given by:

$$\tau_M^{-1} = \pi \frac{\Delta v}{\sqrt{2}} \tag{4}$$

Furthermore [48]:

$$\tau_M^{-1} = \frac{k_B T}{h} e^{\frac{-\Delta G^{\#}}{RT}} \tag{5}$$

where k_B is the Boltzmann constant, R is the gas constant and $\Delta G^{\#}$ the free energy of activation. Based on Eqs. (4) and (5), we can

Table 2
Interproton distances in Irinotecan derived from NOESY spectrum.

Interproton NOEs	Distance (nm)[a]	Distance in the monomer
17–18	0.25	0.25
17–8,12	0.54	Variable
17–9,11a′	0.46	Variable
17–9,11a′	0.45	Variable
17–9,11b′	0.53	Variable
18–28	**0.58**	0.68
18–29	0.50	0.47
18–43	0.66	Variable
21–28	**0.47**	0.55
21–8,12	0.63	Variable
21–9,11a′	0.46	Variable
21–9,11a′	0.49	Variable
21–9,11b′	0.48	Variable
28–37	0.32	Variable
28–38	0.38	Variable
29–28	0.56	0.52
29–36	0.51	0.51
29–38	0.68	Variable
29–42	0.42	Variable
29–43	0.41	Variable
36–42	0.37	Variable
36–43	0.65	Variable
41–29	0.34	Variable

[a] Distances involving the exchangeable proton 41 were not considered. Distances in bold differ from the value expected for the monomer.

measure the free energy of activation from the temperature of coalescence T_c by:

$$\Delta G^{\#} = RT_c\left(22.96 + \ln\frac{T_c}{\Delta v}\right) \quad (6)$$

In this case, using a T_c of 328 K and a Δv of 124 Hz, results in a $\Delta G^{\#}$ of 65.3 kJ/mol.

3.3. Effect of concentration on drug stability and aggregation state

Concentrated solutions of Irinotecan (above 1 mM) were found to be stable at room temperature for several weeks. Mass spectrometry of freshly diluted solutions (0.1 mM) of Irinotecan show a well defined peak at m/z equal to 587 (the molecular ion) and 665 (its DMSO adduct) but not at 605, thus excluding the formation of the lactone form. On the contrary, both the NMR and mass spectra of diluted solutions changed substantially after few days, revealing a degradation of Irinotecan, proved by the disappearance of corresponding UV and MS signals at the expected retention times (1.90 min; 4.22 min for the DMSO adduct). New peaks were generated whose interpretation is beyond the scope of this work. However, these data suggest that self-aggregation might take place, protecting the drug from degradation.

In order to understand the causes of the phenomenon, ^{1}H spectra of freshly prepared solutions of Irinotecan at different concentrations were measured (Fig. 3).

No significant variations are observable below 0.125 mM suggesting that the molecule is in the monomeric state in this range of concentrations. ^{13}C spectra also vary with concentration and ^{13}C chemical shift variations were used to guide the molecular modelling of the dimeric form of Irinotecan (see Section 3.6).

Interestingly above 1 mM, the hydroxyl proton in position 41 becomes observable in ^{1}H spectra (Fig. 3) suggesting its possible implication in a hydrogen bond protecting it from exchange with residual water.

3.4. Association constants

Based on the observed changes in chemical shifts as a function of concentration, we determined the association constant by means of the isodesmic model. The model implies that in a self

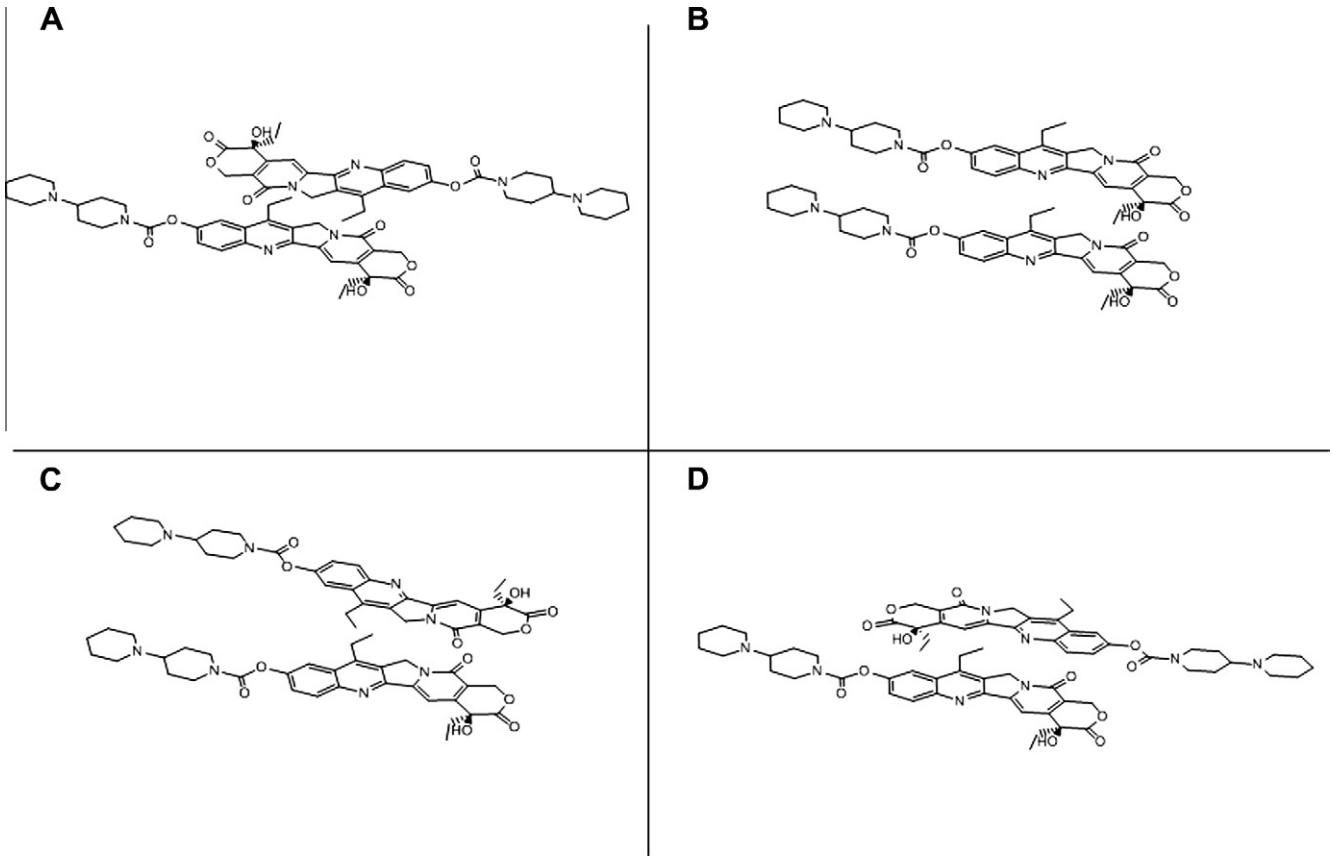

Fig. 7. Four possible relative orientations of Irinotecan monomers allowing stacking of aromatic rings. Figure was created using Chemdraw Ultra 11.0.1.

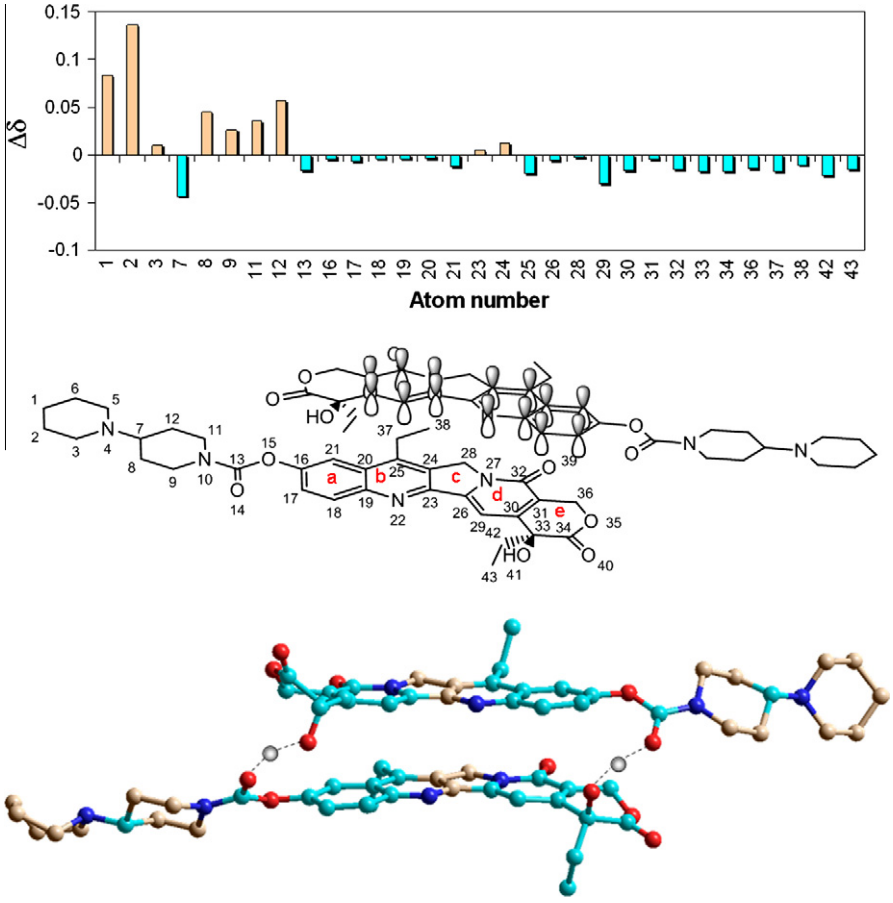

Fig. 8. ^{13}C chemical shift δ variations ($\Delta\delta$) between Irinotecan 20 mM and 12.6 mM. Model D of Fig. 7, shown with atomic orbitals of aromatic regions, fulfils the experimental observations. The sign of ^{13}C chemical shift variation is pictorially displayed onto the molecular structure obtained from energy minimization of the model. Deshielding (ivory) and shielding (violet) effects are highlighted. Atom coloured in blue and red indicate nitrogen or oxygen respectively.

aggregation process each step takes place with the same equilibrium constant. The assumption is physically reasonable, assuming a stacking interaction among the aromatic planes.

The equilibrium constant K of each single step was estimated by plotting the chemical shift of signals belonging to protons 8 and 12 (1.79 ppm at low concentration) as a function of the concentration and fitting the obtained curve with the following equation [49]:

$$\delta^{obs} = \delta^{m} + \Delta_0 K[C][2 - K[C]] \tag{7a}$$

$$[C] = C\left[\frac{2}{1+\sqrt{4KC+1}}\right]^2 \tag{7b}$$

where δ^m is the chemical shift of the monomer, Δ_0 is the limiting deviation of the aggregate from δ^m ($= \delta^{aggr} - \delta^m$), [C] is the equilibrium concentration of the monomer and C is the global concentration of the species. Fig. 4 shows the fitting curve and the obtained value of K for each stage of the aggregation ($5.25 \times 10^2\ M^{-1}$).

This value allows estimating that at 20 mM about 75% of the molecules are associated.

3.5. Diffusion measurements

The formation of aggregates was also monitored by diffusion measurements. The diffusion coefficient D is dependent on the value of the viscosity of the solvent, according to the Stokes–Einstein relation [4]:

$$D = \frac{k_B T}{f_T} \quad f_T = 6\pi\eta r_H \tag{8}$$

where f_T is the friction factor, K_B is the Boltzmann constant, η is the viscosity and r_H is the hydrodynamic radius of the molecule. The diffusion coefficient D of internal trimethylsilyl propionate (TSP) was used to estimate the viscosity of each solution, whose value is required for the determination of the hydrodynamic radius of the aggregates. Given the measured diffusion coefficient and the hydrodynamic radius of TSP (0.351 nm [50]), the viscosity of the solution is calculated using Eq. (8).

The average molecular weight of the species in solutions, calculated as described in Section 2, can be estimated by the diffusion coefficient, provided an estimate of the axial ratio of the aggregates is given. Molecular modelling provided a value of 0.5 for the dimeric form of Irinotecan (see Section 3.6). However, Fig. 5 shows how the apparent molecular weight of the solute is increasing with concentration regardless the value of the axial ratio, thus confirming the self-association phenomenon.

The molecular weight calculated at the highest concentration (using an axial ratio of 0.5) is close to that of a dimer (993 vs. 1174, expected if the entire drug was in dimeric form). The reduced value is due to the fact that the observed diffusion coefficient D contains contributions from the monomeric form of the drug. A better agreement can be obtained taking into account the molar fractions of monomeric and multimeric forms, as follows:

$$D^{associated} = \frac{D^{observed} - D^{monomer} x_{monomer}}{x_{associated}} \tag{9}$$

where x is the molar fraction.

Using Eq. (2), we obtained an apparent molecular weight of 1040 at 6.3 mM which is more compatible with the molecular weight of a dimer (1174). Interestingly, the molecular weight found at 12.6 mM (1350) is larger than what expected for a dimer and may suggest the formation of more sizable (though not extremely large) aggregates at higher concentrations. The presence of small amounts of high mass oligomers in solution could indeed remain hidden in the experimental average of diffusion values as measured by NMR, due to their small diffusion coefficient. On the contrary, when aggregation is observed through relaxation, the presence of high molecular weight species is more easily revealed due to their intrinsically large transversal relaxation rates. However, in the present study both the shape of the molecule and the sign of the chemical shift deviations upon drug concentration, indicate a stacking intermolecular interaction which is well described by the isodesmic model. The calculated value of the association constant derived from the model ($5.25 \times 10^2\ M^{-1}$) suggests that the formation of large aggregates is very unlikely, at least in the experimental conditions studied in this work.

3.6. Intermolecular contacts by NOE

The structural details of the associated form can in principle be inferred by nuclear Overhauser effect (NOE) data of concentrated solutions (20 mM), as the equilibrium constant for association ensure that a significant fraction of the molecule is in associated form at this concentration (74.2%). However, data must be interpreted taking into account that different kind of dimeric species can coexist. As shown in Fig. 6, the NOESY spectrum of Irinotecan displays many expected "medium-range" and a few "long-range" cross peaks compatible with distances beyond 0.55 nm (taken as limiting distance for the observation of intramolecular NOE effects), which could in principle originate intermolecularly. All NOESY-derived interproton distances were calculated as described in Section 2.3 and are reported in Table 2. Most of the distances found are in very good agreement with those expected for a monomer (as if all NOEs were intramolecular). Two distances (namely 21–28 and 18–28, shown as bold lines in Fig. 6) appear to be shorter than expected and may indicate some close intermolecular NOE effect in the dimer. However, the 21–28 NOE could be affected by spin diffusion in the monomer, with protons 37 mediating the magnetization transfer. Given the good agreement found between the calculated and intramolecular distances and the low proton density in the molecule, spin diffusion is unlikely to significantly affect the rest of the data. The NOE between protons 18 and 28 is supposed to be weak, given the relatively large distance separating the two protons in the monomer (their distance is the largest among the fixed ones) and therefore can be affected by larger errors due to spectral noise.

In conclusion, we could not find interprotons NOEs clearly attributable to the dimeric form of Irinotecan and insight in the structural features of the dimer should be searched for in the sign of the ^{13}C chemical shift deviations upon increasing concentrations. The large magnetic anisotropy of aromatic moieties is in fact expected to cause a major shielding effect onto the atoms residing above or under the aromatic plane in a hypothetical Irinotecan dimer. As a matter of facts, most of the carbon atoms in the planar portion of the molecule do experience shielding with increasing concentration and consequent dimer formation. Fig. 7 shows four possible relative orientation of the aromatic planes while the shielding/deshielding effect observed on ^{13}C chemical shift are shown in Fig. 8, suggesting stacking between the aromatic moieties, as proposed previously by Aiyama et al. in water [42].

Out of the possible four relative orientation of the aromatic planes (A–D in Fig. 7), one (D) is better capable to explain the observed effect on chemical shift: shielding of most part of the molecule and deshielding of ring "c" and the flexible piperidino—piperidino moiety. In fact ring "e" cannot face an aromatic region (and thus be shielded) in models B and C while A and D are both compatible with its shielding. In A, however, the stacking surface is poor for sterical reasons and only one ring in each dimer can face an aromatic moiety, while in D both "e" rings have the same chemical environment and this better explains the large shielding effect induced by increased concentration (larger than that observed for rings a and b). As regards the piperidino—piperidino moiety, we observe a large deshielding effect confirming the formation of a stacking interaction. In fact, in the monomer, the piperidino—piperidino moiety is very flexible and its chemical shift reflects shielding contributions from conformations bringing it over the aromatic plane. Upon dimer formation, such conformations are sterically prohibited causing a global deshielding effect on its carbon chemical shift.

The D model was therefore refined by energy-minimization using the Assisted model building with energy refinement (AMBER) force field. The resulting structure is shown in Fig. 8 (bottom). Such structure is actually qualitatively compatible with the observed NOEs, as it does not imply short intermolecular proton–proton distances which would be incompatible with the experimental NOESY spectrum. Moreover, two intermolecular hydrogen bonds are found by energy minimization involving the lactone "e" ring (see Fig. 8), which are able to explain the appearance of the hydroxyl proton in the ^1H NMR spectrum of concentrated Irinotecan (see Section 3.3). Such interaction might also explain the improved stability of concentrated solutions of the drug.

However, the obtained dimer should be simply considered a model as it is based on the sign of ^{13}C chemical shift deviations, which in turn likely result from an ensemble average of many possible intermolecular orientations.

4. Conclusions

The NMR analysis of the solutions of Irinotecan was able to characterize its association process in DMSO solutions. While below a concentration of 1 mM the molecule is mostly monomeric, at higher concentrations it self associates initially forming dimers which are the main species at 20 mM. The data are supported by both ^1H chemical shift and diffusion studies. Structural features of the dimer were inferred by ^{13}C chemical shifts and NOE effect leading to a model implying stacking between the aromatic planes which in turn requires the extrusion of the piperidino—piperidino moieties. The model is compatible with the formation of two intermolecular hydrogen bonds involving the lactone ring "e", which might account for the increased stability of concentrated solution of the drug.

Acknowledgments

We thank Bruker Biospin s.r.l. for providing a 600 MHz spectrometer Bruker Avance III Ultra Shield Plus, CBM (Consorzio per il Centro di Biomedicina Molecolare S.c.r.l., AREA Science Park, Basovizza, Trieste, Italy) for hosting the instrumentation.

References

[1] L.J. Oostendorp, P.F. Stalmeier, P.C. Pasker-de Jong, W.T. Van der Graaf, P.B. Ottevanger, Anticancer Drugs 21 (2010) 749.
[2] J. Weekes, A.K. Lam, S. Sebesan, Y.H. Ho World, J. Gastroenterol. 15 (2009) 3597.
[3] D.R. Spigel, F.A. Greco, J.D. Zubkus, P.B. Murphy, R.A. Saez, C. Farley, D.A. Yardley, H.A. Burris III, J.D. Hainsworth, J. Thorac. Oncol. 4 (2009) 1555.
[4] J.A. Kepler, M.C. Wani, J.N. McNaull, M.E. Wall, S.G. Levine, J. Org. Chem. 34 (1969) 3853.

[5] W. Shou-Fang, H. Pei-Wen, W. Chin-Chung, L. Chia-Lin, C. Shu-Li, L. Chi-Yu, W. Tian-Shung, C. Fang-Rong, Molecules 13 (2008) 1361.
[6] R.H. Mathijssen, R.J. van Alphen, J. Verweij, W.J. Loos, K. Nooter, G. Stoter, A. Sparreboom Clin, Cancer Res. 7 (2001) 2182.
[7] J.G. Slatter, P. Su, J.P. Sams, L.J. Schaaf, L.C. Wienkers, Drug Metab. Dispos. 25 (1997) 1157.
[8] M.C. Haaz, L. Rivory, S. Jantet, D. Ratanasavanh, J. Robert, Pharmacol. Toxicol. 80 (1997) 91.
[9] Y.H. Hsiang, R. Hertzberg, S. Hecht, L.F. Liu, J. Biol. Chem. 260 (1985) 14873.
[10] Y.H. Hsiang, M.G. Lihou, L.F. Liu, Cancer Res. 49 (1989) 5077.
[11] K.W. Kohn, Y. Pommier, Ann. N.Y. Acad. Sci. 922 (2000) 11.
[12] M.C. Wani, A.W. Nicholas, G. Manikumar, M.E. Wall, J. Med. Chem. 30 (1987) 1774.
[13] M.C. Wani, A.W. Nicholas, M.E. Wall, J. Med. Chem. 30 (1987) 2317.
[14] C. Jaxel, K.W. Kohn, M.C. Wani, M.E. Wall, Cancer Res. 49 (1989) 1465.
[15] W. Bocian, R. Kawecki, E. Bednarek, J. Sitkowski, M.P. Williamson, P.E. Hansen, Chemistry 14 (2008) 2788.
[16] B. Ziomkowska, S. Kruszewski, R. Siuda, Opt. Appl. 36 (2006) 137.
[17] I. Chourpa, A. Beljebbar, G.D. Sockalingum, J.F. Riou, M. Manfait Biochim, Biophys. Acta 1334 (1997) 349.
[18] R.P. Hertzberg, M.J. Caranfa, S.M. Hecht, Biochemistry 28 (1989) 4629.
[19] N. Sanna, G. Chillemi, A. Grandi, S. Castelli, A. Desideri, V. Barone, J. Am. Chem. Soc. 127 (2005) 15429.
[20] W.Y. Li, R.T. Koda, Am. J. Health Syst. Pharm. 59 (2002) 539.
[21] T.G. Burke, Z. Mi, Anal. Biochem. 212 (1993) 285.
[22] Z. Mi, T.G. Burke, Biochemistry 33 (1994) 10325.
[23] Y. Tang, P.R. Czuczman, S.T. Chung, A.L. Lewis, J. Control Release 127 (2008) 70.
[24] T.H. Chou, S.C. Chen, I.M. Chu, J. Biosci. Bioeng. 95 (2003) 405.
[25] D.C. Drummond, C.O. Noble, Z. Guo, K. Hong, J.W. Park, D.B. Kirpotin, Cancer Res. 66 (2006) 3271.
[26] B.J. Boyd, D.V. Whittaker, S.M. Khoo, G. Davey, Int. J. Pharm. 318 (2006) 154.
[27] C.L. Messerer, E.C. Ramsay, D. Waterhouse, R. Ng, E.M. Simms, N. Harasym, P. Tardi, L.D. Mayer, M.B. Bally, Clin. Cancer Res. 10 (2004) 6638.
[28] S. Norbedo, F. Dinon, M. Bergamin, S. Bosi, V. Aroulmoji, R. Khan, E. Murano, Carbohydr. Res. 344 (2009) 98.
[29] C. Tripisciano, M.H. Rummeli, X. Chen, Phys. Status Solidi B (2010) 1.
[30] G. Tardi, R.C. Gallagher, S. Johnstone, N. Harasym, M. Webb, M.B. Bally, L.D. Mayer, Biochim. Biophys. Acta 1768 (2007) 678.
[31] A. Dicko, A.A. Frazier, B.D. Liboiron, A. Hinderliter, J.F. Ellena, X. Xie, C. Cho, T. Weber, P.G. Tardi, D. Cabral-Lilly, D.S. Cafiso, L.D. Mayer, Pharm. Res. 25 (2008) 1702.
[32] M. Ramesh, P. Ahlawat, N.R. Srinivas, Biomed. Chromatogr. 24 (2010) 104.
[33] N. Subramanian, S. Sundaraganesan, V. Sudha, G.D. Aroulmoji, M. Sockalingam, Acta A Mol. Biomol. Spectrosc. 78 (2011) 1058.
[34] S. Riahi, S. Eynollahi, M.R. Ganjali, P. Norouzi, Int. J. Electrochem. Sci. 5 (2010) 1151.
[35] B.L. Staker, M.D. Feese, M. Cushman, Y. Pommier, D. Zembower, L. Stewart, A.B. Burgin, J. Med. Chem. 48 (2005) 2336.
[36] B.L. Staker, K. Hjerrild, M.D. Feese, C.A. Behnke, A.B. Burgin Jr., L. Stewart, Proc. Natl. Acad. Sci. USA 99 (2002) 15387.
[37] J.E. Chrencik, B.L. Staker, A.B. Burgin, P. Pourquier, Y. Pommier, L. Stewart, M.R. Redinbo, J. Mol. Biol. 339 (2004) 773.
[38] S. Bencharit, C.L. Morton, E.L. Howard-Williams, M.K. Danks, P.M. Potter, M.R. Redinbo, Nat. Struct. Biol. 9 (2002) 337.
[39] M. Harel, J.L. Hyatt, B. Brumshtein, C.L. Morton, R.M. Wadkins, I. Silman, J.L. Sussman, P.M. Potter, Chem. Biol. Interact. 157–158 (2005) 153.
[40] H.M. Dodds, D.J. Craik, L.P. Rivory, J. Pharm. Sci. 86 (1997) 1410.
[41] H.M. Dodds, J. Robert, L.P. Rivory, J. Pharm. Biomed. Anal. 17 (1998) 785.
[42] R. Aiyama, H. Nagai, S. Sawada, T. Yokokura, H. Itokawa, M. Nakanishi, Chem. Pharm. Bull. 40 (1992) 2810.
[43] C.S. Johnson Jr., Prog. Nucl. Magn. Reson. Spectrosc. 34 (1999) 203.
[44] C.R. Cantor, P.R. Shimmel, Biophysical Chemistry, Part II: Techniques for the Study of Biological Structure and Function, W.H. Freeman, New York, NY, 1980.
[45] S. Yao, G.J. Howlett, R.S. Norton, J. Biomol. NMR 16 (2000) 109.
[46] J. Cavanagh, W.J. Fairbrother, A.G. Palmer III, N.J. Skelton, Protein NMR Spectroscopy. Principles and Practice, Academic Press, Inc, 1996.
[47] A. Hocquet, M. Langgård, J. Mol. Model. 4 (2008) 94.
[48] H. Eyring, J. Chem. Phys. 3 (1935) 107.
[49] T.H. Lilley, H. Linsdell, A. Maestre, J. Chem. Soc. Faraday Trans. 88 (1992) 2865.
[50] E. Gaggelli, F. Berti, N. D'Amelio, N. Gaggelli, G. Valensin, L. Bovalini, A. Paffetti, L. Trabalzini, Environ. Health Perspect. 110 (Suppl 5) (2002) 733.